nature communications

Article

https://doi.org/10.1038/s41467-025-55984-x

Optical signatures of lattice strain in chemically doped colloidal quantum wells

Received: 23 May 2024

Accepted: 3 January 2025

Published online: 18 January 2025

Check for updates

Junhong Yu [1,2] ✉, Hilmi Volkan Demir [2,3] ✉ & Manoj Sharma [2,4] ✉

Lattice strain plays a vital role in tailoring the optoelectronic performance of colloidal nanocrystals (NCs) with exotic geometries. Although optical identifications of lattice strain in irregular-shaped NCs or hetero-structured NCs have been well documented, less is known about optical signatures of the sparsely distributed lattice mismatch in chemically-doped NCs. Here, we show that coherent acoustic phonons (CAPs) following bandgap optical excitations in Cu-doped CdSe colloidal quantum wells (CQWs) offer a unique platform for indirectly measuring the dopant-induced lattice strain. By comparing the behavior of CAPs in Cu-doped and undoped CQWs (i.e., vibrational phase/lifetime/amplitude), we have revealed the driving force of CAPs related to the optical screening of lattice strain-induced piezoelectric fields, which thus allows to determine the strain-induced piezoelectric field of ~10^2 V/m in Cu-doped CdSe CQWs. This work may facilitate a detailed understanding of lattice strain in chemically-doped colloidal NCs, which is a prerequisite for the design of favorable doped colloids in optoelectronics.

Benefitting from the innovation of solution-processed synthesis techniques, colloidal semiconductor nanocrystals with exotic geometries (e.g., irregular-shaped[1,2], hetero-structured[3,4], and chemically doped[5,6]) have been developed. These exotic geometries with unique band structure and carrier dynamics offer a great opportunity for expanding the optoelectronic properties of colloidal nanocrystals (NCs), which have already found applications in diverse optoelectronic applications, with earlier examples showing, for instance, continuous-wave lasing in biaxial asymmetry colloidal quantum dots (CQDs)[7], ultralong-lived indirect exciton in CdSe/CdS colloidal rod-in-rods[8], and near-unity dopant emission efficiency in Cu-doped CdSe colloidal quantum wells (CQWs)[6]. Generally, it is agreed that peculiar optoelectronic properties of colloidal NCs with exotic geometries are set by quantum confinement via the NC size[9], band offset through the growth of heterostructures[10], or localized electronic states in chemical doping[11].

Recent studies have revealed that inherent lattice strain in colloidal NCs with exotic geometries, which are naturally grown under large lattice mismatch conditions, could also play a considerable role in bandgap engineering and carrier dynamics manipulation[12–15]. As a result, the ability to visualize or measure crystal lattice strain of colloidal NCs with exotic geometries, which is essential to fully understand optoelectronic properties, has been receiving considerable attention in the evolving research framework. For irregular-shaped or hetero-structured colloidal NCs, the lattice strain at the particle level or at the nanoscale interface can be directly visualized based on the high-resolution transmission electron microscopy using the peak pairs analysis[8,16] or indirectly measured based on emission/absorption properties using ultrafast[17,18] and steady-state spectroscopy[19–21]. Nevertheless, these methodologies are incapable or at least insufficient to visualize or measure lattice strain in chemically doped colloidal NCs due to the sparse distribution of lattice mismatch at the atomic level[19,20].

To fill in the gap, we report ultrafast coherent phonon measurements in Cu-doped CdSe CQWs, which provides a unique way to probe nonequilibrium lattice vibrations and thus allows to detect the dynamics of lattice strain. We show that the behavior of coherent

[1]College of Physics and Electronic Engineering, Chongqing Normal University, Chongqing, China. [2]LUMINOUS! Centre of Excellence for Semiconductor Lighting and Displays, School of Electrical and Electronic Engineering, Nanyang Technological University, Singapore, Singapore. [3]Department of Electrical and Electronics Engineering and Department of Physics, UNAM-Institute of Materials Science and Nanotechnology, Bilkent University, Ankara, Turkey. [4]ARC Centre of Excellence in Exciton Science, Department of Materials Science and Engineering, Monash University, Melbourne, VIC, Australia.
✉e-mail: jyu012@e.ntu.edu.sg; hvdemir@ntu.edu.sg; manoj.sharma@monash.edu

acoustic phonons (CAPs) in Cu-doped CdSe CQWs contrasts strikingly with the behavior of CAPs in undoped counterparts triggered by displacive excitation, including a π/2 vibrational phase shift, a prolonged vibrational lifetime, and a distinct wavelength-/fluence-dependent vibrational behavior. We corroborate the anomalous CAPs in Cu-doped CdSe CQWs with the optical screening of lattice strain-induced piezoelectric fields, which is driven by the trapping of excited holes to the Cu^{1+} state on a vibrationally impulsive time scale. Based on the damped driven harmonic oscillator model and the experimental oscillation amplitudes, we have extracted a strain-induced piezoelectric field of ~10^2 V/m in Cu-doped CdSe CQWs, which is several orders of magnitude smaller than the intrinsic piezo response of wurtzite CdSe/CdS heterostructures.

Results

Undoped CdSe CQWs with a vertical thickness of 1.2 nm corresponding to four monolayers (MLs) of lattice unit are synthesized according to reported procedures[22,23], and copper ions doped into CdSe CQWs are achieved by using the nucleation doping method[6,24–26]. The average number of copper dopants per CQW ($\langle N_{Cu} \rangle$), which is determined by inductively coupled plasma-mass spectrometry (ICP-MS)[6,27], is about 40 in the investigated sample (i.e., ~0.3% concerning Cu/Cd atomic concentration). As shown in Fig. 1a, copper dopants modify neither the geometry of the CQWs (i.e., Cu-doped and undoped CQWs possess an approximately rectangular shape with a uniform size distribution as presented in their transmission electron micrographs, with the size distribution curves given in Fig. S1) nor the essential excitonic absorbance of the CQWs (i.e., the electron/heavy-hole transition at ~512 nm and electron/light-hole transition at ~481 nm remain unchanged). Here, the role of copper dopants is reflected in two aspects: (i) Copper ions introduce emissive midgap states into the CQW host, manifesting as a broad reddish emission band in the photoluminescence profile and a broad absorption tail on the red side of the heavy-hole excitonic feature. As schematically shown in Fig. 1b, Cu has the electronic structure $(Ar)3d^{10}4s^1$ in its neutral state, and Cu ions introduced into the CdSe CQW as substitutional defects have the $(Ar)3d^{10}$ configuration (Cu^{1+}). After photoexcitation, copper dopants quickly localize the photogenerated holes in the host, Cu^{1+} is promoted to Cu^{2+} with the configuration of $(Ar)3d^9$ and therefore activated as a radiative acceptor for the CB electrons. The copper emission process can be expressed as: $[Ar]3d^9 + e \rightarrow [Ar]3d^{10} + h\nu$. Meanwhile, the sub-band-gap Cu^{1+} to CB transition is also allowed, which manifests in the absorption spectrum as a broad absorption tail on the red side of the heavy-hole excitonic feature. Please note that the stable ground state of copper dopants as Cu^{1+} is supported by transient absorption measurements, PL excitation spectroscopy, and X-ray photoelectron spectroscopy[6,28]. (ii) The replacement of cadmium ions with copper ions breaks the lattice periodicity and lattice contraction (i.e., a symmetric contraction or a Jahn–Teller distortion[28,29]) is favored to stabilize the dopant-host lattice (see Fig. 1c), resulting in a sparse distribution of lattice strain at the atomic level. Such a sparsely distributed lattice strain would give rise to polarization along the Cu–Se bond direction, which translates into the local piezoelectric field[8,30].

When copper ions are introduced into the CQW lattice, unique lattice vibrational dynamics related to the lattice strain have been predicted[29]. To verify this, we have utilized femtosecond-resolved coherent phonon spectroscopy[31–33] at room temperature (i.e., 298 K) to compare the nonequilibrium phonon behavior of Cu-doped and undoped CdSe CQWs (experimental details are presented in Methods). To avoid contributions of the Auger-mediated carrier trapping process[33], the fluence of the 400 nm pump pulse is set to be ~5.69 μJ/cm^2, corresponding to an initial averaged exciton population $\langle N_0 \rangle$ of ~0.37[34] (see the evaluation process of $\langle N_0 \rangle$ in "Methods" and Fig. S2). The probed pulse is centered at the electron/heavy-hole transition (~512 nm), and the pure response of coherent lattice vibrations at room temperature is presented in Fig. 1d, in which the non-oscillation signal related to photoexcited carriers has been subtracted. It can be seen that the lattice vibration of Cu-doped CQWs has a time-domain spectrum that is highly similar to that of undoped CQWs, except for the subtle waving at long time windows. Frequencies of these time-domain oscillations are clarified from the Fourier transform (FT)[31,35] and the resulting power spectra, with frequencies in units of THz, are shown in Fig. 1e. For both Cu-doped and undoped CQWs, FT spectra exhibit a dominant high-frequency mode at ~6.2 THz (Cu-doped: 6.24 THz or 208.2 cm^{-1}; Undoped: 6.22 THz or 207.7 cm^{-1}) and a low-frequency mode at ~0.6 THz (Cu-doped: 0.64 THz or 21.3 cm^{-1}; Undoped: 0.65 THz or 21.8 cm^{-1}). Based on previous Raman measurements[36,37], the higher frequency oscillation corresponds to the longitudinal–optical (LO) phonon of CdSe CQWs, while the lower frequency oscillation is assigned to the longitudinal acoustic (LA) phonon of CdSe CQWs. Please note that the acoustic phonon propagation in CdSe CQWs is anisotropic[35,36]. In the vertical direction, the acoustic phonon mode creates a one-dimensional standing wave to deform the unit cell (similar to the case of CQDs), and across the lateral directions, acoustic phonons propagate compression waves (similar to the case of bulk materials). Interestingly, a stronger acoustic phonon oscillation is identified in Cu-doped CQWs, which may imply an additional driving force for lattice vibrations considering the similar excitation condition for doped/undoped CQWs[38].

To quantify the difference of lattice vibrations in Cu-doped and undoped CQWs, we have fitted the time-domain oscillations in Fig. 1d using a sum of two damped sinusoidal functions[31,33,39]:

$$\frac{\Delta R}{R0}(t) = \sum_{i=1}^{2} A_i \sin(\omega_i t + \phi_i) \exp\left(\frac{t}{\tau_i}\right) \quad (1)$$

where A_i, ω_i, τ_i, and ϕ_i are the amplitude, frequency, lifetime, and initial phase of the i^{th} oscillation component, respectively. As shown in the upper panel of Fig. 2, the temporal oscillations can be well-described by Eq. 1 with a good agreement between the extracted ω and oscillation frequencies obtained in FT power spectra, confirming the reliability of the fitting process (the fitting residual and fitting parameters are provided in Fig. S3). Figure 2 also shows the contributions of individual oscillation components that are reconstructed from the fitting parameters. The high-frequency LO phonon at ~6.2 THz in Cu-doped and undoped CQWs (the lower panel of Fig. 2) are very similar with an initial phase closely approaching π/2 rad (Cu-doped: 0.477 π; Undoped: 0.482 π), indicative of the phonon driving force as typical displacive excitation (i.e., ultrafast laser excitation of the electronic system makes atoms displaced from the equilibrium state and coherently oscillated around the new nonequilibrium position)[40]. In contrast, the acoustic phonon at ~0.6 THz in Cu-doped CQWs shows an abrupt phase shift of nearly π/2 compared to that in undoped CQWs (Cu-doped: 0.054 π; Undoped: 0.461 π) and this anti-phased vibrational wavepacket of the acoustic phonon in Cu-doped CQWs suggests again a different driving force[41,42]. Please note that the initial phase is determined at the minimum time delay point (t^*) when experimental data starts to deviate from the damped oscillation fitting and the time point t^* has been manually set as zero for better clarity of initial phases of the waves (e.g., the cosine-like and the sine-like oscillations), which can be seen more clearly in the linear plot in Fig. S4. In addition, we have noticed that the lifetime of acoustic phonons is prolonged for Cu-doped CQWs (Cu-doped: 4.26 ps; Undoped: 1.73 ps), implying that the driving force of acoustic phonons in Cu-doped CQWs may related to the dopant-induced lattice strain (i.e., lattice contraction in Cu-doped CQWs improves Young's modulus, resulting in an enhanced acoustic phonon group velocity and suppressed acoustic phonon anharmonic decaying[28,43]).

A general mechanism other than displacive excitation responsible for the generation of coherent acoustic phonons in colloidal NCs includes impulsive stimulated Raman scattering and impulsive lattice

https://doi.org/10.1038/s41467-025-55984-x

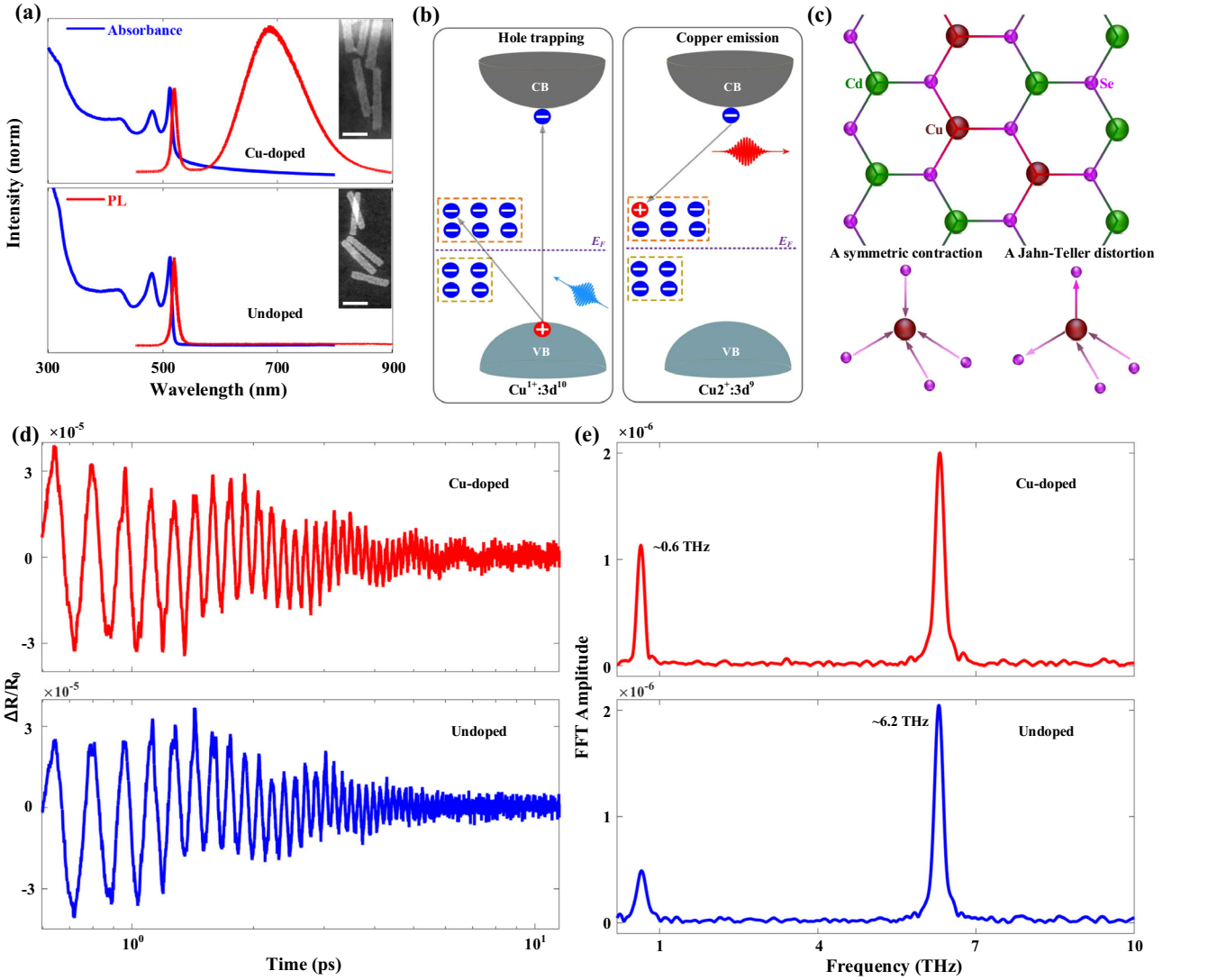

Fig. 1 | Basic properties and coherent phonon spectra of doped and undoped CQWs. a Steady-state absorption and emission profiles of Cu-doped (upper panel) and undoped (lower panel) 4 ML CdSe CQWs. The inset is a transmission electron micrograph with a scale bar of 20 nm. **b** Schematics illustrating the carrier transitions and radiative recombination in copper-doped CdSe CQWs. CB conduction band, VB valence band, E_F Fermi level. **c** A schematic of lattice strain in Cu-doped CdSe CQWs with two types of Cu–Se bond distortions. The overall distortion can be approximated by the sum of distortions along totally symmetric (left part of the bottom panel) and T_2 Jahn–Teller nuclear coordinates (right part of the bottom panel). **d** Semilog plots of time-domain lattice vibrations of Cu-doped (upper panel) and undoped (lower panel) CdSe CQWs with λ_{probe} of 512 nm and $\langle N_O \rangle$ of 0.37. **e** Fourier transform spectrum of the time-domain lattice vibrations in (**d**), showing the longitudinal–optical phonon mode at ~6.2 THz and the longitudinal acoustic phonon mode at ~0.6 THz.

heating. Since the pump pulse in our experiments is not negatively chirped, a significant impulsive stimulated Raman contribution is ruled out[44]. Meanwhile, we have estimated the lattice temperature increase in Cu-doped CQWs based on the two-temperature model (see the estimation details in Supplemental Note 1) and the lattice temperature rise of ~18.6 K is much smaller than that required to drive coherent phonons by impulsive lattice heating (e.g., ~10^3 K in metal NCs[45]). The exclusion of general driving forces for coherent acoustic phonons concentrates our focus on the intrinsic difference between Cu-doped and undoped CQWs: the introduction of copper dopants. Inspired by coherent oscillations generated by surface charge trapping induced piezoelectric response in CdSe CQDs[32,35], we consider the possibility that the ultrafast hole trapping in Cu^{1+} ions could provide the impulse for driving coherent acoustic phonons in Cu-doped CQWs. The hole trapping partially screens the local piezoelectric field at copper ions such that an ensuing sudden lattice expansion occurs along the Cu–Se bond direction[32,45]. Consequently, the heavy ionic nuclei find themselves out of equilibrium and start to oscillate around their new position in phase with each other. It is worth noting that this physical picture in Cu-doped CQWs could also reasonably explain the π/2 phase shift (i.e., the displacive excitation generates a wavepacket on the excited-state potential energy surface which starts to propagate but then the hole trapping shifts the propagating direction and projects the wavepacket to the trapped-state potential energy surface[33,46]) and the immune LO phonon behavior (i.e, the hole trapping time in Cu-doped CQWs of >4 ps[47–49] is much longer than the LO phonon oscillation periods $T = 2\pi/\omega_{LO} \approx 1$ ps, violating the condition for the impulsive excitation[50]). The proposed generation mechanism has been further supported by lattice vibrations in Cu-doped CQWs with different doping concentrations (see Fig. S5 and Table S1 for details), in which an enhanced oscillation amplitude, a more abrupt phase change to 0, and a prolonged oscillation lifetime are identified in CQWs with a larger $\langle N_{Cu} \rangle$.

We have performed probe wavelength-dependent measurements to gain deeper insights into the lattice strain-mediated coherent phonon behaviors in Cu-doped CQWs. Figure 3a, b shows time-domain

https://doi.org/10.1038/s41467-025-55984-x

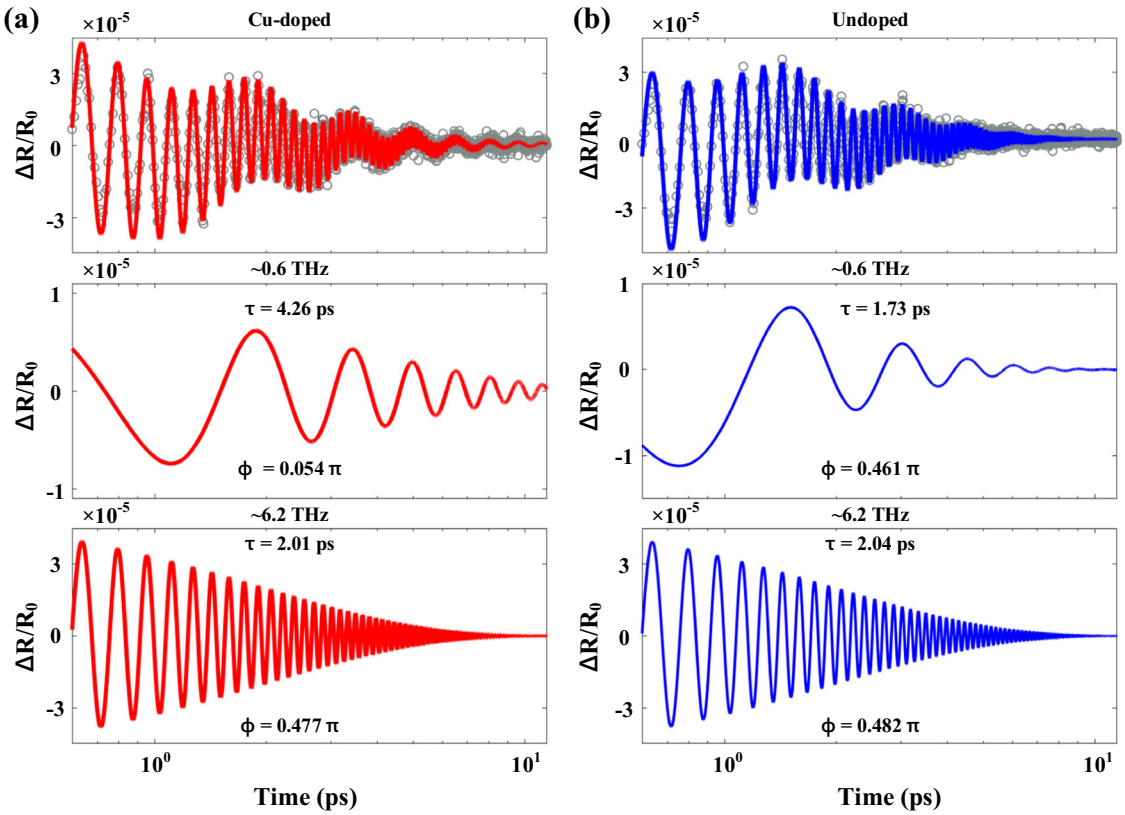

Fig. 2 | Analyzing coherent phonon behaviors in doped and undoped CQWs. **a** Two damped sinusoidal functions fitting of time-domain lattice vibrations of Cu-doped CdSe CQWs with λ_{probe} of 512 nm and $<N_O>$ of 0.37. Upper panel: Semilog plot of the overall fitting; middle panel: Semilog plot of the fitted longitudinal acoustic phonon mode; lower panel: Semilog plot of the fitted longitudinal–optical phonon mode. **b** Two damped sine functions fitting of time-domain lattice vibrations of undoped CdSe CQWs with λ_{probe} of 512 nm and $<N_O>$ of 0.37. Upper panel: Semilog plot of the overall fitting; middle panel: Semilog plot of the fitted longitudinal acoustic phonon mode; lower panel: Semilog plot of the fitted longitudinal–optical phonon mode.

oscillations of Cu-doped and undoped CQWs with $<N_0>$ of ~0.37 at three representative probe wavelengths (e.g., 504 nm, 512 nm, 520 nm). The full set of coherent phonon spectra of Cu-doped and undoped CQWs with probe wavelengths ranging from 504 to 520 nm can be found in Figs. S6 and S7. Corresponding FT power spectra of Cu-doped and undoped CQWs versus probe wavelength are depicted in a 2D plot (see Fig. 3c), in which the amplitude dependence on the probe wavelength is well displayed, as marked by the red star in Fig. 3c. It can be seen that for both phonon modes in undoped CQWs and the LO phonon mode in Cu-doped CQWs, the amplitude shows a maximum at ~512 nm, which matches the wavelength of the electron/heavy-hole transition in the 4 ML CdSe CQW host; while for the acoustic phonon (~0.6 THz) in Cu-doped CQWs, the amplitude is relatively independent of the probe wavelength. To clarify the origin of these probe wavelength dependences, we have normalized the phonon amplitude at λ_{probe} = 512 nm and plotted it with the scaled absorbance spectra in Fig. 3d. We have revealed that amplitudes of both phonon modes in undoped CQWs and the LO phonon mode in Cu-doped CQWs follows the absorbance in a good manner, which is a clear fingerprint of the displacive excitation mechanism (i.e., the oscillation amplitude of coherent phonons launched by displacive excitation is essentially reflecting the exciton-phonon coupling strength and therefore, strong coherent oscillations are observed at probed spectral positions where the electronic resonance is large[51,52]). In the case of the acoustic phonon in Cu-doped CQWs, the nearly unchanged amplitude around the electron/heavy-hole transition can be intuitively rationalized with the proposed generation mechanism. The oscillation amplitude of coherent phonons triggered by hole trapping process is mainly related to the optical screening strength of lattice strain-induced piezoelectric fields (i.e., the number of trapped holes at copper ions on a vibrationally impulsive time scale[53,54]), resulting in an insensitive acoustic oscillation with varying probe wavelength.

To further validate the different driving forces of acoustic phonons in Cu-doped and undoped CQWs, we have conducted pump fluence-dependent measurements at a probe wavelength of 512 nm. Figure 4a, b shows time-domain oscillations of Cu-doped and undoped CQWs with three representative initial exciton populations (e.g., $<N_0>$ of ~0.37, ~2.73, ~6.46). The full set of coherent phonon spectra of Cu-doped and undoped CQWs with $<N_0>$ ranging from ~0.37 to ~6.46 can be found in Figs. S8 and S9. As shown in Fig. 4c, d, the acoustic phonon amplitude and phase in Cu-doped and undoped CQWs show a distinct behavior with varying $<N_0>$. For the acoustic phonon driven by optical screening of the local piezoelectric field (i.e., the Cu-doped CQWs), the driven force should be proportional to the hole population trapped at the Cu^{1+} dopant site, leading to a linearly increasing acoustic phonon amplitude. With $<N_0>$ larger than ~3.33, the phonon amplitude becomes gradually saturated due to the limited dopant population, which is further supported by the $<N_0>$-dependent copper emission measurement (see Fig. S10, the copper emission saturates with a similar $<N_0>$).

For the acoustic phonon in undoped CQWs, displacive excitation should also result in a linearly increased phonon amplitude (i.e., generated phonon populations through electron-phonon coupling are linearly dependent on the excitation fluence[55]). With $<N_0>$ larger than ~1.57, accelerated amplitude enhancement is consistent with the recent result of Dong et al.[33] and can be attributed to the Auger-mediated acoustic phonon generation process (i.e., the ultrafast Auger process in undoped CQWs transfers the vibrational coherence of excited-state

https://doi.org/10.1038/s41467-025-55984-x

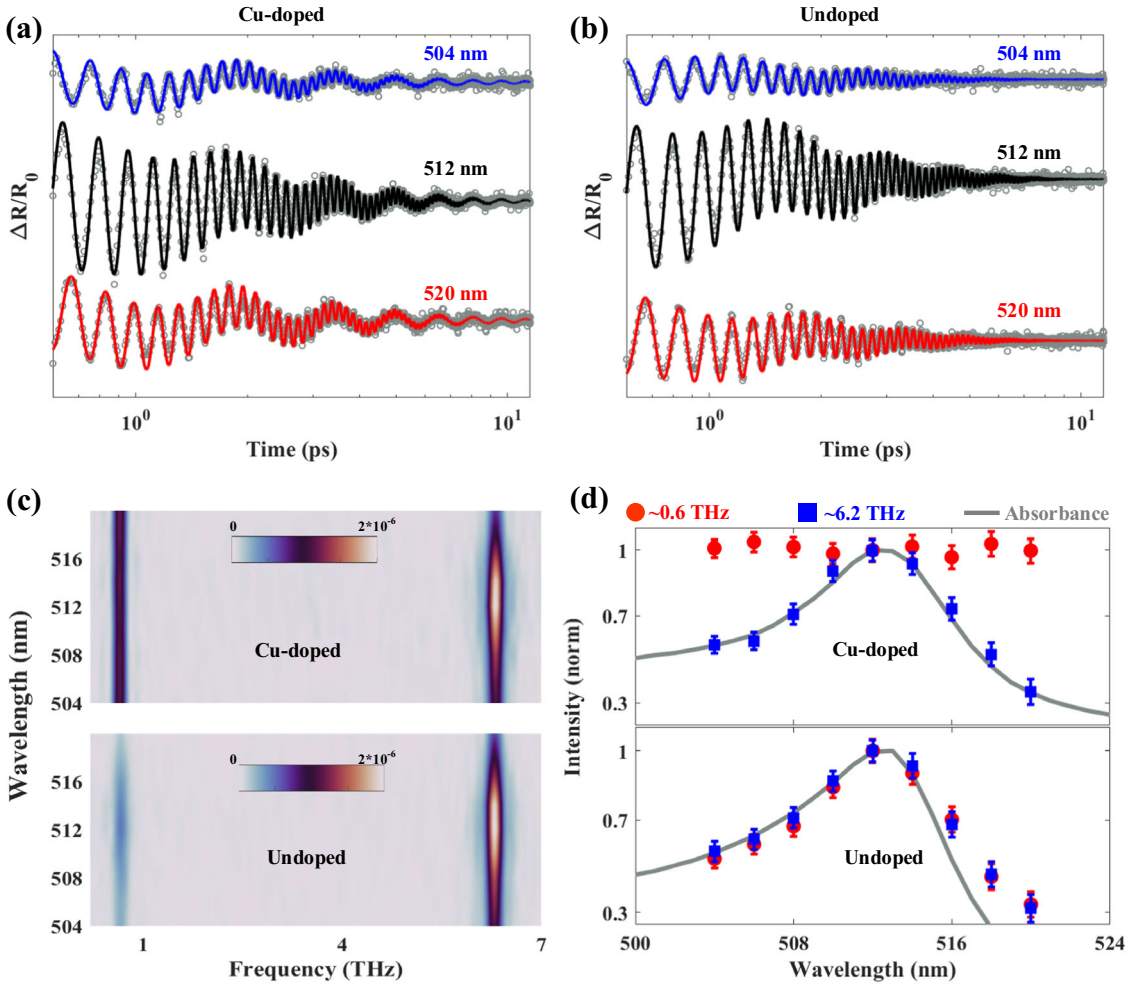

Fig. 3 | Wavelength-dependent coherent phonon spectra of doped and undoped CQWs. a Semilog plots of time-domain lattice vibrations of Cu-doped CdSe CQWs with $\langle N_O \rangle$ of 0.37 and different λ_{probe}. **b** Semilog plots of time-domain lattice vibrations of undoped CdSe CQWs with $\langle N_O \rangle$ of 0.37 and different λ_{probe}. **c** 2D contour plot of λ_{probe}-dependent amplitudes of coherent phonon modes in Cu-doped (the upper panel) and undoped (the lower panel) CQWs with $\langle N_O \rangle$ of 0.37. **d** Scaled absorbance curve and the normalized λ_{probe}-dependent coherent phonon amplitudes of Cu-doped (upper panel) and undoped (lower panel) CdSe CQWs with $\langle N_O \rangle$ of 0.37. The error bars are estimated based on the uncertainties of FFT amplitudes.

populations to the high-energy state and launches the coherent lattice vibration). Meanwhile, the coherent phonon phase following the Auger process should be shifted based on the appearance of vibrational wavepackets on high-energy states, which is also manifested in our measurements (see the π-phase jump with $\langle N_O \rangle$ around 2 in the lower panel of Fig. 4d). Please note that due to the suppressed Auger recombination[25,47], the contribution of Auger-mediated coherent acoustic phonons generation at high excitation fluence in Cu-doped CQWs is negligible, as evident by the absence of phase jump and the amplitude increase trend. In addition, we have conducted pump fluence-dependent measurements with different doping concentrations (e.g., $\langle N_{Cu} \rangle$ of 5 and $\langle N_{Cu} \rangle$ of 70) at a probe wavelength of 512 nm. As shown in Fig. S11, $\langle N_O \rangle$-dependent behavior of the CAP amplitude and phase in Cu-doped CQWs using different doping concentrations also supports the main conclusion of our works: the trapping of excited holes to the Cu^{1+} state on a vibrationally impulsive time scale screens lattice strain-induced piezoelectric fields, triggering the coherent acoustic phonon oscillation.

Discussion

Different from previous works[31,32,52], we are viewing CAPs from a largely different perspective and focusing on utilizing the behavior of CAPs as an indicator of intrinsic lattice strains in Cu-doped CQWs. After confirming the dominant lattice strain-mediated acoustic phonon generation in Cu-doped CQWs, we could determine the driving force based on a phenomenological damped harmonic oscillator model[56–58]:

$$\mu\left(\frac{d^2Q(t)}{dt^2} + 2\gamma\frac{dQ(t)}{dt} + \omega^2 Q\right) = F(t) \quad (2)$$

where μ is the reduced lattice mass, γ is the phonon dephasing rate, ω is the coherent acoustic phonon frequency, and F is the driving force originating from screening of the piezoelectric field. By converting the oscillated reflectivity change ($\Delta R/R$) into the atomic displacement (Q)[59] and relating the driving force (F) to the screened piezoelectric field[57], the amplitude of the screened piezoelectric electric field in Cu-doped CQWs with $\langle N_O \rangle$ of ~6.46 (i.e., in the saturation regime) is determined to be ~1.72×10^2 V/m (detailed calculation process is provided in Supplementary Note 2), which is several orders of magnitude smaller than reported values in irregular-shaped colloidal NCs or heterostructured colloidal NCs (e.g., 1.5×10^7 V/m in CdSe/CdS rod-in-rod NCs[8] and 7×10^7 V/m in CdSe/CdS dot-in-rod NCs[19]). Although this estimation only reflects an average value of the local piezoelectric field within our excitation spot (e.g., with a diameter at FWHM of ~120 μm) and phenomenological assumptions (e.g., assuming the atomic displacement is isotropic, assuming the physical constants are time-

https://doi.org/10.1038/s41467-025-55984-x

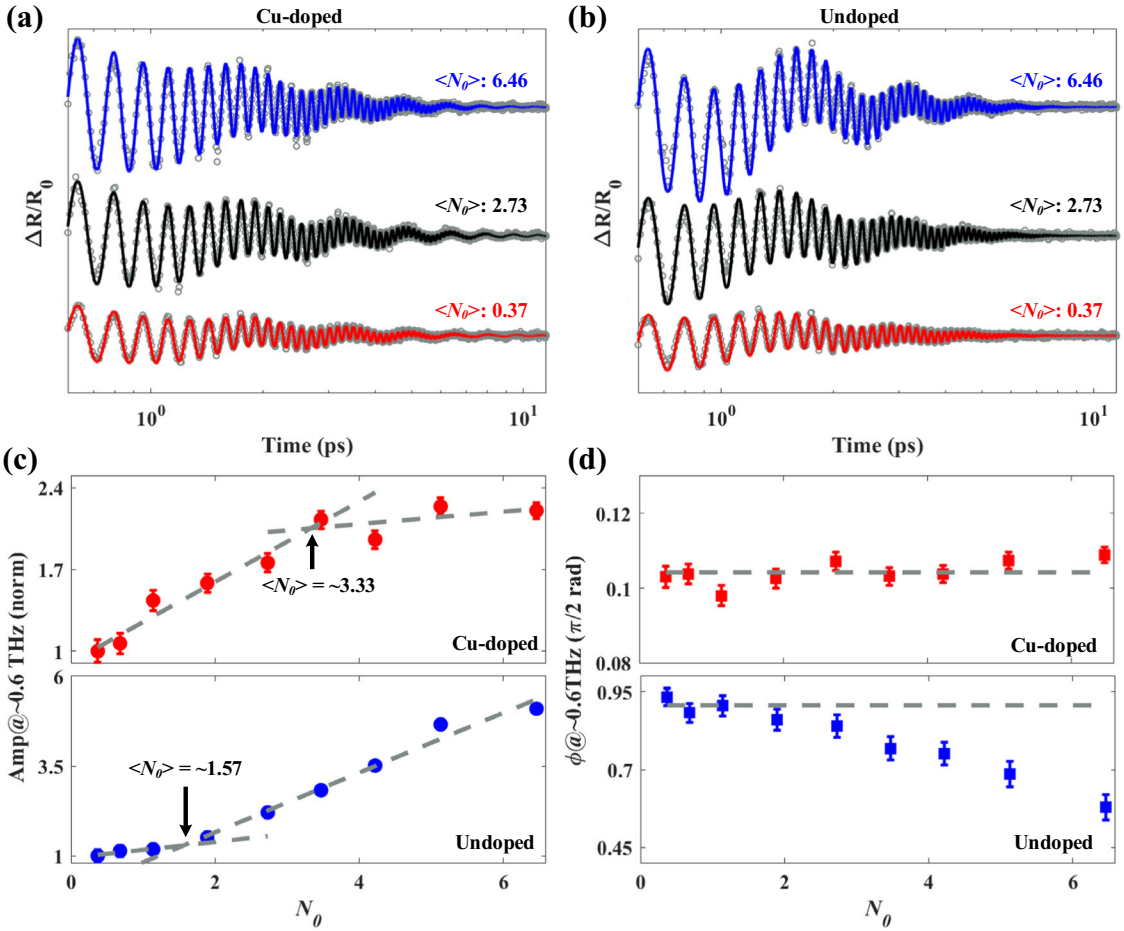

Fig. 4 | Fluence-dependent coherent phonon spectra of doped and undoped CQWs. a Semilog plots of time-domain lattice vibrations of Cu-doped CdSe CQWs with λ_{probe} of 512 nm and different $<N_0>$. **b** Semilog plots of time-domain lattice vibrations of undoped CdSe CQWs with λ_{probe} of 512 nm and different $<N_0>$. **c** $<N_0>$-dependent amplitudes of the longitudinal acoustic phonon mode in Cu-doped (upper panel) and undoped (lower panel) CQWs. The dashed lines are linear fittings. The error bars are estimated based on the uncertainties of FFT amplitudes. **d** $<N_0>$-dependent phases of the longitudinal acoustic phonon mode in Cu-doped (upper panel) and undoped (lower panel) CQWs. The dashed lines are guidelines. The error bars are estimated based on the uncertainties of the damped sinusoidal fittings.

independent, and ignoring the contribution of displacive excitations) in the estimation process also reduces the evaluation accuracy in Cu-doped CdSe CQWs, we argue that coherent phonons generated via optical screening of the piezoelectric field should be a general physical picture in colloidal NCs with exotic geometries, which could provide a feasible route to evaluate the lattice strain down to the atomic level.

In principle, our method which is based on ultrafast optical screenings of local piezoelectric fields to estimate the lattice strain in chemically doped colloidal nanocrystals should have a certain extent of generalizability to other dopants besides copper since it is inevitable that the replacement of host ions with dopants could break the lattice periodicity (i.e., symmetry breaking) and lead to the local piezoelectric fields[5,11]. As shown in Fig. S13, the coherent acoustic phonons in Ag-doped CQWs also contrast the case in undoped CQWs and show fingerprints of driving by the trapping of excited holes to the Ag^{1+} state[48,60] on a vibrationally impulsive time scale, including a π/2 vibrational phase shift (~0.02 π) and a prolonged vibrational lifetime (~5.6 ps). However, we need to also point out that this method has its limitations considering the following: (i) photoexcited carriers should interact with dopants via trapping or dipole-dipole interactions to screen the local piezoelectric field at dopant ions such that ensuing sudden lattice expansion occurs; (ii) piezoelectric fields induced driving force should satisfy the "impulsive limit", which is the limit effective when the time scale of the driving force is less than a single vibrational oscillation period, otherwise, the coherent lattice vibrations will be immune to the screening of piezoelectric fields; and (iii) strong enough pump fluences are required to generate photocarriers to saturate the dopants for an accurate evaluation of lattice strain. Therefore, although we have proposed a feasible optical approach to evaluate the lattice strain in chemically doped colloidal nanocrystals, future efforts are further needed to expand its generalizability to different doping systems.

In summary, ultrafast coherent phonon spectroscopy elucidates the behavior of coherent acoustic phonon in Cu-doped and undoped CdSe CQWs following optical bandgap excitations. CAPs in undoped CdSe CQWs can be well-described by the typical displacive excitation mechanism while the acoustic phonon oscillations in Cu-doped CdSe CQWs are launched via optically induced piezoelectric coupling to the CdSe lattice, which enables the experimental detection of dopant-induced lattice strain within the framework of the damped harmonic oscillator description. Our understanding of CAP behavior and the proposed optical evaluation of lattice strain create opportunities for precisely modulating the optoelectronic properties in chemically doped colloidal semiconductor nanocrystals.

Methods

Sample synthesis and characterization. Four ML core-only undoped CdSe CQWs are synthesized according to our previously published

method[22,23]. Four ML core-only Cu-doped CdSe CQWs were also synthesized according to the previously published literature[6,24–26]. All synthesized samples are cleaned with ethanol to remove excess ligands and finally dispersed in hexane for further experiments and measurements. The absorption spectra of doped and undoped CQWs in hexane are measured by an ultraviolet–visible spectrophotometer (Shimadzu, UV-1800). The PL of doped and undoped CQWs are recorded using a spectrofluorophotometer (Shimadzu, RF-5301PC, excitation wavelength for PL: 355 nm).

Coherent phonon measurements. The nonequilibrium lattice vibration dynamics of Cu-doped and undoped CdSe CQWs at room temperature are measured by conducting the nondegenerate pump-probe experiment using a cavity-dumped Ti: sapphire layer. The pump pulse at a center wavelength of 400 nm is generated by frequency doubling the fundamental 800 nm pulse with a beta barium borate (BBO) crystal, which has a duration of ~20 fs at a repetition rate of 400 kHz, while the probe pulse is generated from an optical parametric amplifier (Coherent OPerA Solo) pumped by a 1 kHz regenerative amplifier (Coherent Libra, 800 nm, 50 fs). The polarization of the pump pulse and the probe pulse is set orthogonal to each other to eliminate the coherent artifact. A neutral density filter is used to control the pump power for the fluence dependence study. The pump and probe pulses are focused on the sample at the near-normal incidence and the measurements are performed in a transmission geometry. The time delay between the pump and probe beam is varied using a retroreflector mounted on a delay stage.

Calculations of excitons per CQW $<N>$. The average number of excitons per CQWs ($<N_0>$) is calculated by $<N_0> = f\sigma/(\hbar\omega)$, where f is the pump fluence, σ is the absorption cross-section at 400 nm, and $\hbar\omega$ is the excitation photon energy. Since the Cu-doped CQWs involve the hole trapping process, it is unsuitable to determine the absorption cross-section by the state-filling effect assuming the Poisson distribution. Instead, here we evaluate the absorption cross-section of Cu-doped and undoped CQWs based on the empirical equation reported previously by our group, where A is the absorbance, C_{CQW} is the concentration, NA is the Avogadro's number, and L is the optical path length. Inductively coupled plasma-mass spectroscopy (ICP-MS) measurement is used to calculate the concentration of Cu-doped and undoped CQWs. By obtaining the cadmium and copper molar concentrations (C_{Cd+Cu}), we can obtain $C_{CQW} = C_{Cd+Cu} \times V\text{unit}/(4V_{CQW})$, where Vunit is the volume of the CdSe unit cell and V_{CQW} is the physical volume of a CQW. As a result, absorption cross-sections of 3.23×10^{-14} cm^2 and 2.74×10^{-14} cm^2 are obtained for the Cu-doped and undoped CQWs, respectively.

Reporting summary

Further information on research design is available in the Nature Portfolio Reporting Summary linked to this article.

Data availability

The main data presented and analyzed in this project are contained within the article and supplementary information. The data generated in this study are provided with this paper in the source data file. Source data are provided with this paper.

References

1. Fiore, A. et al. Tetrapod-shaped colloidal nanocrystals of II-VI semiconductors prepared by seeded growth. *J. Am. Chem. Soc.* **131**, 2274–2282 (2009).
2. Deka, S. et al. Octapod-shaped colloidal nanocrystals of cadmium chalcogenides via "one-pot" cation exchange and seeded growth. *Nano Lett.* **10**, 3770–3776 (2010).
3. Bae, W. K. et al. Controlled alloying of the core–shell interface in CdSe/CdS quantum dots for suppression of auger recombination. *ACS Nano* **7**, 3411–3419 (2013).
4. Mahler, B., Nadal, B., Bouet, C., Patriarche, G. & Dubertret, B. Core/shell colloidal semiconductor nanoplatelets. *J. Am. Chem. Soc.* **134**, 18591–18598 (2012).
5. Norris, D. J., Efros, A. L. & Erwin, S. C. Doped nanocrystals. *Science* **319**, 1776–1779 (2008).
6. Sharma, M. et al. Near-unity emitting copper-doped colloidal semiconductor quantum wells for luminescent solar concentrators. *Adv. Mater.* **29**, 1700821 (2017).
7. Fan, F. et al. Continuous-wave lasing in colloidal quantum dot solids enabled by facet-selective epitaxy. *Nature* **544**, 75–79 (2017).
8. Christodoulou, S. et al. Band structure engineering via piezoelectric fields in strained anisotropic CdSe/CdS nanocrystals. *Nat. Commun.* **6**, 7905 (2015).
9. Smith, A. M. & Nie, S. Semiconductor nanocrystals: structure, properties, and band gap engineering. *Acc. Chem. Res.* **43**, 190–200 (2010).
10. Celso de Mello, D. Synthesis and properties of colloidal heteronanocrystals. *Chem. Soc. Rev.* **40**, 1512–1546 (2011).
11. Buonsanti, R. & Milliron, D. J. Chemistry of doped colloidal nanocrystals. *Chem. Mater.* **25**, 1305–1317 (2013).
12. Smith, A. M., Mohs, A. M. & Nie, S. Tuning the optical and electronic properties of colloidal nanocrystals by lattice strain. *Nat. Nanotechnol.* **4**, 56–63 (2009).
13. Yang, S., Prendergast, D. & Neaton, J. B. Strain-induced band gap modification in coherent core/shell nanostructures. *Nano Lett.* **10**, 3156–3162 (2010).
14. Kim, D., Shcherbakov-Wu, W., Ha, S. K., Lee, W. S. & Tisdale, W. A. Uniaxial strain engineering via core position control in CdSe/CdS core/shell nanorods and their optical response. *ACS Nano* **16**, 14713–14722 (2022).
15. Park, Y.-S., Lim, J. & Klimov, V. I. Asymmetrically strained quantum dots with non-fluctuating single-dot emission spectra and subthermal room-temperature linewidths. *Nat. Mater.* **18**, 249–255 (2019).
16. Galindo, P. L. et al. The peak pairs algorithm for strain mapping from HRTEM images. *Ultramicroscopy* **107**, 1186–1193 (2007).
17. Wu, K. et al. Efficient and ultrafast formation of long-lived charge-transfer exciton state in atomically thin cadmium selenide/cadmium telluride type-II heteronanosheets. *ACS Nano* **9**, 961–968 (2015).
18. McDaniel, H., Pelton, M., Oh, N. & Shim, M. Effects of lattice strain and band offset on electron transfer rates in type-II nanorod heterostructures. *J. Phys. Chem. Lett.* **3**, 1094–1098 (2012).
19. Morello, G. et al. Intrinsic optical nonlinearity in colloidal seeded grown cdse/cds nanostructures: photoinduced screening of the internal electric field. *Phys. Rev. B* **78**, 195313 (2008).
20. Rainò, G. et al. Probing the wave function delocalization in CdSe/CdS dot-in-rod nanocrystals by time- and temperature-resolved spectroscopy. *ACS Nano* **5**, 4031–4036 (2011).
21. Bryan, J. D. & Gamelin, D. R. Doped semiconductor nanocrystals: synthesis, characterization, physical properties, and applications. *Prog. Inorg. Chem.* **54**, 47–126 (2005).
22. Ithurria, S. et al. Colloidal nanoplatelets with two-dimensional electronic structure. *Nat. Mater.* **10**, 936–941 (2011).
23. Ithurria, S. & Dubertret, B. Quasi 2D colloidal cdse platelets with thicknesses controlled at the atomic level. *J. Am. Chem. Soc.* **130**, 16504–16505 (2008).
24. Sharma, M. et al. Understanding the journey of dopant copper ions in atomically flat colloidal nanocrystals of CdSe nanoplatelets using partial cation exchange reactions. *Chem. Mater.* **30**, 3265–3275 (2018).
25. Yu, J. et al. Low-threshold lasing from copper-doped CdSe colloidal quantum wells. *Laser Photonics Rev.* **15**, 2100034 (2021).
26. Yu, J. et al. Modulating emission properties in a host–guest colloidal quantum well superlattice. *Adv. Opt. Mater.* **10**, 2101756 (2022).
27. Poitrasson, F. & Freydier, R. Heavy iron isotope composition of granites determined by high resolution MC-ICP-MS. *Chem. Geol.* **222**, 132–147 (2005).

28. Yu, J. et al. Observation of phonon cascades in Cu-doped colloidal quantum wells. *Nano Lett.* **22**, 10224–10231 (2022).
29. Nelson, H. D., Li, X. & Gamelin, D. R. Computational studies of the electronic structures of copper-doped CdSe nanocrystals: oxidation states, Jahn-Teller distortions, vibronic bandshapes, and singlet-triplet splittings. *J. Phys. Chem. C.* **120**, 5714–5723 (2016).
30. Huong, N. Q. $Mn2^{+}$ emission in mn-doped quantum dots. In *Nano-Sized Multifunctional Materials* (ed Nguyen, H. H.) 47–71 (Elsevier, 2019).
31. Schnitzenbaumer, K. J. & Dukovic, G. Comparison of phonon damping behavior in quantum dots capped with organic and inorganic ligands. *Nano Lett.* **18**, 3667–3674 (2018).
32. Tyagi, P. et al. Controlling piezoelectric response in semiconductor quantum dots via impulsive charge localization. *Nano Lett.* **10**, 3062–3067 (2010).
33. Dong, S., Lian, J., Jhon, M. H., Chan, Y. & Loh, Z.-H. Pump-power dependence of coherent acoustic phonon frequencies in colloidal CdSe/CdS core/shell nanoplatelets. *Nano Lett.* **17**, 3312–3319 (2017).
34. Yeltik, A. et al. Experimental determination of the absorption cross-section and molar extinction coefficient of colloidal CdSe nanoplatelets. *J. Phys. Chem. C.* **119**, 26768–26775 (2015).
35. Dworak, L., Matylitsky, V. V., Braun, M. & Wachtveitl, J. Coherent longitudinal-optical ground-state phonon in CdSe quantum dots triggered by ultrafast charge migration. *Phys. Rev. Lett.* **107**, 247401 (2011).
36. Cherevkov, S. A., Fedorov, A. V., Artemyev, M. V., Prudnikau, A. V. & Baranov, A. V. Anisotropy of electron-phonon interaction in nanoscale CdSe platelets as seen via off-resonant and resonant Raman spectroscopy. *Phys. Rev. B* **88**, 041303(R) (2023).
37. Kudlacik, D. et al. Single and double electron spin-flip Raman scattering in CdSe colloidal nanoplatelets. *Nano Lett.* **20**, 517–525 (2020).
38. Thomsen, C. et al. Coherent phonon generation and detection by picosecond light pulses. *Phys. Rev. Lett.* **53**, 989–992 (1984).
39. Jeong, T. Y. et al. Coherent lattice vibrations in mono- and few-layer WSe_2. *ACS Nano* **10**, 5560–5566 (2016).
40. Zeiger, H. J. et al. Theory for displacive excitation of coherent phonons. *Phys. Rev. B* **45**, 768–778 (1992).
41. Yamamoto, A., Mishina, T. & Masumoto, Y. Coherent oscillation of zone-folded phonon modes in GaAs-AlAs superlattices. *Phys. Rev. Lett.* **73**, 740 (1994).
42. Kim, J. H. et al. Chirality-selective excitation of coherent phonons in carbon nanotubes by femtosecond optical pulses. *Phys. Rev. Lett.* **102**, 037402 (2009).
43. Liu, C. et al. Unexpected doping effects on phonon transport in quasi-one-dimensional van der Waals crystal TiS_3 nanoribbons. *Nat. Commun.* **14**, 5597 (2023).
44. Bardeen, C. J., Wang, Q. & Shank, C. V. Selective excitation of vibrational wave packet motion using chirped pulses. *Phys. Rev. Lett.* **75**, 3410–3413 (1995).
45. Hartland, G. V. Coherent excitation of vibrational modes in metallic nanoparticles. *Annu. Rev. Phys. Chem.* **57**, 403–430 (2006).
46. Malkmus, S. et al. Chirp dependence of wave-packet motions in oxazine. *J. Phys. Chem. A* **109**, 10488–10492 (2005).
47. Yu, J. et al. Efficient generation of emissive many-body correlations in copper-doped colloidal quantum wells. *Cell Rep. Phys. Sci.* **3**, 101049 (2022).
48. Khan, A. H. et al. Tunable and efficient red to near-infrared photoluminescence by synergistic exploitation of core and surface silver doping of CdSe nanoplatelets. *Chem. Mater.* **31**, 1450–1459 (2019).
49. Medda, A. et al. Impacts of dopant and post-synthetic heat-treatment on carrier relaxation of Cu2+-doped CdSe nanoplatelets. *J. Phys. Chem. C.* **126**, 7739–7747 (2022).
50. Sun, C.-K., Liang, J.-C. & Yu, X.-Y. Coherent acoustic phonon oscillations in semiconductor multiple quantum wells with piezoelectric fields. *Phys. Rev. Lett.* **84**, 179 (2000).
51. Lueer, L. et al. Coherent phonon dynamics in semiconducting carbon nanotubes: a quantitative study of electron-phonon coupling. *Phys. Rev. Lett.* **102**, 127401 (2009).
52. Sagar, D. M. et al. Size dependent, state-resolved studies of exciton-phonon couplings in strongly confined semiconductor quantum dots. *Phys. Rev. B: Condens. Matter Mater. Phys.* **77**, 1–14 (2008).
53. Rieger, S., Fürmann, T., Stolarczyk, J. K. & Feldmann, J. Optically induced coherent phonons in bismuth oxyiodide (BiOI) nanoplatelets. *Nano Lett.* **21**, 7887–7893 (2021).
54. Yu, J. et al. Ultrafast control of the optical transition in type-II colloidal quantum wells. *ACS Photonics* **10**, 1250–1258 (2023).
55. Wu, A. Q., Xu, X. & Venkatasubramanian, R. Ultrafast dynamics of photoexcited coherent phonon in Bi_2Te_3 thin films. *Appl. Phys. Lett.* **92**, 011108 (2008).
56. Bragas, A. V. et al. Ultrafast optical generation of coherent phonons in $CdTe_{1-x}$sex quantum dots. *Phys. Rev. B* **69**, 205306 (2004).
57. Pfeifer, T., Dekorsy, T., Kütt, W. & Kurz, H. Generation mechanism for coherent LO phonons in surface-space-charge fields of III-V-compounds. *Appl. Phys. A: Solids Surf.* **55**, 482 (1992).
58. Fu, J. et al. Electronic states modulation by coherent optical phonons in 2D halide perovskites. *Adv. Mater.* **33**, 2006233 (2021).
59. Katsuki, H. et al. All-optical control and visualization of ultrafast two-dimensional atomic motions in a single crystal of bismuth. *Nat. Commun.* **4**, 2801 (2013).
60. Liu, B. et al. Management of electroluminescence from silver-doped colloidal quantum well light-emitting diodes. *Cell Rep. Phys. Sci.* **3**, 100860 (2022).

Acknowledgements

J.Y. acknowledges financial support from the National Natural Science Foundation of China under Grant 12304032&62205041, also acknowledges support from the National Key Research and Development Program (2023YFB3611100); H.V.D. acknowledges financial support in part from the Singapore Agency for Science, Technology and Research (A*STAR) MTC program under grant number M21J9b0085, Ministry of Education, Singapore, under its Academic Research Fund Tier 1 (MOE-RG62/20) and in part from TUBITAK 119N343, 20AG001, 121N395, and 121C266. H.V.D. also acknowledges support from TUBA and TUBITAK 2247—A National Leader Researchers Program (121C266).

Author contributions

J.Y. initiated the project and performed the ultrafast coherent phonon experiment. M.S. synthesized the high-quality doped and undoped CdSe CQWs. J.Y., M.S., and H.V.D. analyzed the results and wrote the manuscript.

Competing interests

The authors declare no competing interests.

Additional information

Supplementary information The online version contains supplementary material available at https://doi.org/10.1038/s41467-025-55984-x.

Correspondence and requests for materials should be addressed to Junhong Yu, Hilmi Volkan Demir or Manoj Sharma.

Peer review information *Nature Communications* thanks the anonymous reviewer(s) for their contribution to the peer review of this work. A peer review file is available.